Physics of Fluids

Numerical investigation of wavy and spiral Taylor-Görtler vortices in medium spherical gaps

Li Yuan

Citation: Phys. Fluids **24**, 124104 (2012); doi: 10.1063/1.4772196
View online: http://dx.doi.org/10.1063/1.4772196
View Table of Contents: http://pof.aip.org/resource/1/PHFLE6/v24/i12
Published by the American Institute of Physics.

PHYSICS OF FLUIDS **24**, 124104 (2012)

Numerical investigation of wavy and spiral Taylor-Görtler vortices in medium spherical gaps

Li Yuan[a)]
LSEC and NCMIS, Academy of Mathematics and Systems Science, Chinese Academy of Sciences, Beijing 100190, China

(Received 15 July 2012; accepted 15 November 2012; published online 27 December 2012)

The spherical Couette flow between two concentric spheres with only the inner sphere rotating is simulated by solving the 3D incompressible Navier-Stokes equations with a fifth order upwind compact finite difference method. Two moderate clearance ratios, $\beta = (R_2 - R_1)/R_1 = 0.14$ and 0.18, respectively, are chosen for comparison with previous experimental and numerical results. First, the spiral Taylor-Görtler (TG) vortex flow at Re = 1110 for $\beta = 0.14$ [W. M. Sha and K. Nakabayashi, "On the structure and formation of spiral Taylor-Görtler vortices in spherical Couette flow," J. Fluid Mech. **431**, 323–345 (2001)] is found to develop traveling waves at Re = 1800. A wavy TG vortex flow formed at low Re numbers can return to steady TG vortex as Re number is increased to a critical value Re = 6600, thus confirming the occurrence of a reverse Hopf bifurcation from limit cycle to fixed point [K. Nakabayashi, W. M. Sha, and Y. Tsuchida, "Relaminarization phenomena and external-disturbance effects in spherical Couette flow," J. Fluid Mech. **534**, 327–350 (2005)]. Second, multiple supercritical flows for $\beta = 0.18$ [M. Wimmer, "Experiments on a viscous fluid flow between concentric rotating spheres," J. Fluid Mech. **78**, 317–335 (1976)] are simulated for a wide range of Re numbers from the first instability (Re ≈ 655) up to the proximity of transition to turbulence (Re ≈ 8000). The simulation confirms Wimmer's experimental observation that a periodic 2-vortex flow coexists with the steady 0- and 1-vortex flows in certain low Re range. There is also a reverse Hopf bifurcation for this periodic wavy 2-vortex flow at Re = 2270. As Re number is further increased, the steady 0- and 2-vortex flows begin to form spiral waves in the secondary flow region for Re ≥ 6500, while the 1-vortex flow has similar spiral disturbances for Re = 8000. Multiple higher modes with different numbers of spiral waves can be generated by using different wavenumbers in the imposed perturbation. Detailed description of these multiple higher modes is given in terms of rotational frequency, wavenumber, and spatial structure. © *2012 American Institute of Physics*. [http://dx.doi.org/10.1063/1.4772196]

I. INTRODUCTION

The spherical Couette flow (SCF) between two concentric rotating spheres can give rise to a rich variety of flow structures and instability mechanisms in the laminar-turbulent transition. Geometrically, a spherical shell can be considered as a combination of two other simpler systems with cylindrical annulus near the equator and parallel disks in the pole region, thus SCF is similar to the circular Couette flow near the equatorial region, and to the flow between two rotating disks in a stationary housing near the polar region. SCF is an important template for studying various mechanisms of the laminar-turbulent transition of rotating fluid in enclosed cavity, and is also relevant to engineering applications like bearings and gyroscopes (Wimmer[1]).

a) lyuan@lsec.cc.ac.cn.

In this paper we consider the SCF with the inner sphere rotating and the outer sphere stationary. Superficially, there are two control parameters that determine various flow regimes: a Reynolds number $\mathrm{Re} = \Omega R_1^2/\nu$ and a clearance ratio $\beta = (R_2 - R_1)/R_1$, with ν the kinematic viscosity, Ω the angular velocity of the inner sphere, and R_1 and R_2 the radii of the inner and outer spheres. In fact, other factors such as initial conditions, rotational acceleration rate, and perturbations imposed, may also have impact on the formation of different flow disturbances (structures) when the control parameters (Re, β) are located in bifurcation regimes. A lot of studies were conducted on SCF in the past (Sawatzki and Zierep,[2] Munson,[3] Wimmer,[4] Yavorskaya,[5] Bartels,[6] Nakabayashi *et al.*,[7,8] Bühler,[9] Shrauf,[10] Marcus,[11] and Yuan[12]) and a rich variety of distinct flow modes were identified. In a recent work,[13] Nakabayshi *et al.* categorized known disturbances of SCF into two types: a cylinder-type that is similar to that in the circular Couette flow, and a disk-type that is similar to that in the flow between two rotating disks in a stationary housing. Furthermore, they also found several new types of disturbances which are specific to SCF, such as ring vortices, letter-X-like waves, twists, and internal waves within toroidal Taylor-Görtler (TG) vortices.[14] It is well known that toroidal TG vortices, spiral TG vortices, and traveling waves on TG vortices are cylinder-type disturbances, while Stuart vortices and shear waves are disk-type disturbances. Different types of disturbances and their characteristics strongly depend on the clearance ratio β. The Taylor instability in the form of axisymmetric and toroidal Taylor vortices occurs as the first instability for narrow gaps and medium gaps,[3,10,11] while the cross-flow instability in the form of spiral waves or spiral vortices occurs as the first instability for wide gaps (Dumas,[15] Egbers,[16] Zikanov,[17] Araki,[18] Wulf,[19] and Sha[20]). Reference 13 divided β into four regions in the gross. The narrow-gap region refers to $\beta \le \beta_N \approx 0.1$–$0.13$ for which cylinder-type disturbances such as spiral TG vortices and traveling waves play an important role. An intermediate-gap region is particularly delineated as $0.13 \le \beta \le \beta_I \approx 0.17$ for which the spiral TG vortices or traveling waves occurring after the second instability will disappear with increasing Re number (reverse Hopf bifurcation, also called "relaminarlization phenomenon" in Ref. 21, i.e., the disappearance of velocity fluctuation with increasing Re). The medium-gap region refers to $\beta_I \le \beta \le \beta_W \approx 0.3$ for which there is absence of spiral TG vortices and traveling waves, yet disk-type disturbances such as Stuart vortices and shear waves occur at high Re. The wide-gap region refers to $\beta > 0.3$ for which the cross-flow instability (spiral waves or spiral vortices) instead of the Taylor instability occurs as the first instability.

A well-known feature of SCF is that a variety of distinct flow modes, or the same flow mode but with different subcharacteristics such as wavenumbers and modulations can occur at the same supercritical Re number. The most famous example is the coexistence of multiple steady-state Taylor vortex flows with different numbers of vortices at a low Re number. This multiplicity is due to bifurcations of solutions of the Navier-Stokes (NS) equations (cf. Ladyzhenskaya[22]). Previous experiments have shown that the formation of multiple flow modes depends on initial conditions and the Reynolds number history.[4,8] Experiments have obtained multiple Taylor vortex flows,[2,4] multiple traveling waves on TG vortices,[5,8] multiple shear waves with different wavenumbers, and rotational frequencies.[9] Experimental techniques used to generate these multiple flow states include different accelerations of the inner sphere, different initial flow modes, and different perturbations such as temporary rotation of the outer sphere in the same or opposite direction. The characteristics of many higher flow modes were described in a series of papers by Nakabayashi and coauthors.[7,8,13,14,20,21]

Numerical studies of SCF, on the other hand, have only obtained steady multiple flow modes with axisymmetric toroidal TG vortices via either time marching methods[6,11,12] or bifurcation methods (Shrauf,[10] Mamun and Tuckerman[23]), and a few higher modes such as spiral TG vortices[15,20] and shear waves[17,18,24] via time stepping approaches. A careful numerical exploration[20] was carried out to reveal structure and formation mechanism of the spiral TG vortices. However, a wide range of Re numbers needs to be explored in order to clarify abundant experimental findings such as the coexistence of periodic flows with steady flows at the same lower Re number[4] and the reverse Hopf bifurcation, and to further obtain multiple higher flow modes and reveal how they develop into turbulence. In a broader sense, knowledge of transition to turbulence in SCF will be helpful in establishing a general hydrodynamic transition map for rotating flow in enclosed domain.

The objective of the present study is to investigate multiple flow solutions of SCF with only the inner sphere rotating and their development with increasing Re number, especially the occurrence of the reverse Hopf bifurcation and the multiple periodic solutions in moderate gap widths. In a previous study,[24] we implemented the artificial compressibility method in conjunction with a third-order upwind compact finite difference for solving the three-dimensional incompressible NS equations in general curvilinear coordinates system. The computed supercritical steady TG vortex flows were found in good agreement with literature. But for unsteady multiple flows, we found that the formation of higher disturbances needs much longer evolution time and appropriate choice of initial conditions and artificial perturbations. Besides, high-order accuracy of the numerical scheme and mesh independent study are generally required. All these will incur huge computational cost such that it is not easy to make systematic simulation.

In this paper, we adopt a fifth-order accurate upwind compact scheme (Abdullah[25]) for the flow solution, and more notably, we parallelize the code with MPI so that it can run many cases in feasible time. After successfully reproducing the spiral TG vortices for the clearance ratio $\beta = 0.14$ in Ref. 20, we investigate the development of the flow in this β with increasing Re number up to the range in which a reverse Hopf bifurcation happens. Then we revisit the medium gap $\beta = 0.18$ which corresponds to Wimmer's experiment.[4] Multiple higher flow modes for Re ≥ 6500 are simulated after long evolution time. Further, it will be shown that the wavenumber of the artificial perturbation used plays an important role in generating multiple spiral waves in the flows. Our simulation reproduces for the first time Wimmer's experimental result that a periodic double TG vortex flow can coexist with multiple steady TG vortex flows in a lower Re number range. Development of spiral waves (shear waves) imposed on the TG vortex flows for higher Re numbers are explored systematically in terms of fundamental and rotational frequencies, wavenumbers, and spatial structures.

II. NUMERICAL METHOD AND COMPUTATIONAL SETUP

A. Numerical method

The computational domain is an annulus between two concentric spheres filled with an incompressible Newtonian fluid with constant density and kinematic viscosity ν. The inner sphere is constrained to rotate around the vertical axis from west to east with a prescribed angular velocity Ω, while the outer sphere is stationary. The artificial compressibility method is used to solve the three-dimensional incompressible NS equations. The dual-time stepping technique is used to obtain time-accurate solution. The convective terms and the viscous terms are discretized with the fifth-order upwind compact scheme and the second-order central difference scheme, respectively. The discretized equations are solved with the diagonalized Beam-Warming scheme. The detail of the numerical scheme and its parallel implementation can be found in Refs. 25 and 26.

B. Computational setup

The spherical annulus is divided into a number of grids in the radial (r), circumferential (θ), and azimuthal (ϕ) directions, respectively. The grids are uniform in the circumferential and azimuthal directions, but are clustered near both walls in the radial direction. In Ref. 20, grid numbers $22(r) \times 361(\theta) \times 91(\phi)$ were found sufficient to resolve the spiral TG vortex flow for the gap $\beta = 0.14$ at Re $= 1110$. In this work, we use grid numbers $21 \times 361 \times 129$ for reproducing the result in Ref. 20, and $34 \times 512 \times 201$ for higher Re number for the gap $\beta = 0.14$, and $34 \times 360 \times 153$ and $34 \times 480 \times 257$ for the gap $\beta = 0.18$. The nondimensional physical time step $\Delta t = \Delta \tilde{t} \Omega = 0.01$ is used. The pseudo-time marching is implemented with approximate Newton iteration by setting the pseudo-time step to infinity. The subiteration process (pseudo-time marching) is terminated when L_2 norm of the residuals drops 10^{-3} from its initial magnitude or when the subiteration number exceeds 20.

On inner and outer spheres, non-slip conditions are applied to velocities, and the pressure is obtained by the radial component momentum equation written in spherical coordinates. The numerical boundary condition on the polar axis is treated by setting values on the axis equal to averaging neighboring points next to the axis. A reference pressure is taken at a fixed point in the interior of the computational domain.

An important issue associated with numerical simulation of multiple solutions of SCF is the dependence of final solutions on initial conditions, time history of Re number (equivalent to angular acceleration of the inner sphere in experiment), and artificial perturbation imposed. We adopt a form of perturbation similar to that used by Schroeder and Keller[27] to trigger traveling waves of the circular Couette flow:

$$\begin{aligned} v_r &= -4\varepsilon_1 \frac{(r-R_1)(r-R_2)}{(R_2-R_1)^2}\cos\left[\pi\left(1-\frac{2z}{\Gamma}-\varepsilon_2\alpha\right)\right], \\ v_\theta &= \varepsilon_1 \sin\left[\frac{\pi}{2}\frac{(r-R_1)(r-R_m)(r-R_2)}{(R_2-R_1)^3}\right]\sin\left[\pi\left(1-\frac{2z}{\Gamma}-\varepsilon_2\alpha\right)\right]\frac{1}{\beta}, \end{aligned} \tag{1}$$

where $z = R_m\left(\frac{\pi}{2}-\theta\right)$, $R_m = 0.5(R_1+R_2)$, $\alpha = \sin(m_a\phi)$, and $\Gamma = 2(R_2-R_1)$ is roughly the wavelength of the TG vortex in the circumferential direction. The perturbation amplitude ε_1 for velocities is set to 10^{-4}, and the perturbation amplitude ε_2 for the azimuthal variation is set to 0.4 as Ref. 27. Different azimuthal wavenumbers m_a will be used for generating different patterns of spiral waves. Perturbation (1) is used for computing spiral waves for $\beta = 0.18$, which is imposed either at $t = 0$ only, or for a duration of viscous diffusion time across the gap $t_d = (R_2-R_1)^2/\nu$.

III. RESULTS

Two clearance ratios, $\beta = 0.14$ and 0.18, are selected to be the same as those studied by Nakabayashi *et al.*[20,21] and Wimmer,[4] respectively. According to the category of Ref. 13, these two ratios fall into so-called intermediate-gap and medium-gap regions, respectively (see the Introduction). The Reynolds numbers in this study cover $900 \leq \mathrm{Re} \leq 6600$ for $\beta = 0.14$ and $650 \leq \mathrm{Re} \leq 8000$ for $\beta = 0.18$, respectively.

For convenience of discussion, notations used by Ref. 13 are adopted in the following context. The flow regime is characterized by "flow region I, II, III, and IV" + "kinds of disturbances," where flow region I is a laminar basic flow region, II is a TG vortex flow region, III is a transitional flow region, and IV is a turbulent flow region. The kinds of disturbances refer to vortices and waves in the flow, such as TG vortex (T), spiral vortex (S), traveling waves (W), shear waves ($\mathrm{S_h}$), Stuart vortices ($\mathrm{S_u}$), etc. The flow regime is further classified by the flow state expressed in terms of the cell number of toroidal TG vortices N (the pair number $T = N/2$ is more frequently used, denoted as T-vortex), the pair number of spiral vortices S_P, and the wavenumber of traveling waves on TG vortices m, that of shear waves S_H or Stuart vortices S_U. For example, IITS($T = 1$, $S_P = 3$) refers to the spiral TG vortex flow studied in Ref. 20. If the numbers of spirals are different in the northern and southern hemispheres, then the numbers of the spiral vortices/waves in the northern and southern hemispheres are separated by a colon, e.g., IIIWTS($N = 2$, $m = 5$, $S_P = 3$:2) indicates a transitional 2-cell TG vortex flow with 5 wavenumbers for azimuthal traveling waves, and 3 and 2 spiral vortices in the northern and southern hemispheres, respectively.

A. $\beta = 0.14$

For this clearance ratio, Taylor instability in the form of steady 1-vortex flow IIT($T = 1$) occurs first in the equatorial region with increasing Re number.[7,20] The 1-vortex flow has an inflow ($u_r < 0$) boundary between the two toroidal TG vortices at the equator.[4] The occurrence of the 1-vortex flow is related to the presence of symmetry-breaking bifurcation.[10,11] In three-dimensional simulation, round-off errors intricately contain non-equatorially symmetric and nonaxisymmetric perturbations. It is easy to produce the 1-vortex flow for $900 \leq \mathrm{Re} \leq 990$ by computing from either rest or Stokes flow, where $\mathrm{Re}_{c1} \approx 900$ (determined with a resolution $\Delta\mathrm{Re} = 10$) is the critical Reynolds number for the onset of the TG vortex. Once produced, the 1-vortex flow will remain stable for $900 \leq \mathrm{Re} < 1090$, where $\mathrm{Re}_{c2} \approx 1090$ is the Hopf bifurcation point at which the steady 1-vortex flow becomes periodic spiral TG vortex IITS($T = 1$, $S_P = 3$). On the other hand, we can obtain the steady 2-vortex flow IIT($T = 2$) easily for $1000 \leq \mathrm{Re} \leq 1540$ by computing from either rest or Stokes flow. The lower bound $\mathrm{Re} \approx 1000$ for the 2-vortex flow is not a bifurcation point as explained in Ref. 11, while the upper bound $\mathrm{Re}_{c3} \approx 1540$ is a Hopf bifurcation point at which the steady 2-vortex flow becomes a wavy TG vortex flow.

To compare with literature, we reproduce the spiral TG vortex flow at Re = 1110 which was first computed by Sha *et al.*[20] Re number is increased quasi-statically with the same acceleration as that in Ref. 20 ($dR^*/dt = 0.0006$, where R^* is defined as $R^* = \mathrm{Re}/\mathrm{Re}_{c1}$). The initial condition is the 1-vortex flow at Re = 940, and the mesh number used is $21 \times 361 \times 129$ close to $21 \times 361 \times 91$ used in Ref. 20. As Re number is gradually increased to Re = 1110, the flow becomes unstable due to exceeding the secondary instability point $\mathrm{Re}_{c2} = 1090$. After a long transitional time, a completely periodic spiral TG vortex flow with three pairs of spiral vortices is established (IITS($T = 1$, $S_P = 3$)). Figures 1(a)–1(d) show time sequences of (ϕ, θ)-plane distributions of the azimuthal vorticity component, $\omega_\phi = \frac{1}{r}\left[\frac{\partial(r u_\theta)}{\partial r} - \frac{\partial u_r}{\partial\theta}\right]$. This quantity is integrated along the radial direction over the gap. The figures are projected onto the (ϕ, θ)-plane in Cartesian coordinates and plotted over the range $0^\circ \leq \phi \leq 360^\circ$ and $50^\circ \leq \theta \leq 130^\circ$. The four instants, $t = 108\pi$, 227π, 239π, and 277π, are nearly the same as those in Figures 10(a)– 13(a) in Ref. 20. We see that the time scenario is comparable.

We further see how the spiral TG vortex flow (IITS($T = 1$, $S_P = 3$)) evolves for higher Re number. The mesh number used is $34 \times 512 \times 201$. Re number is increased from 1110 ($R^* = 1.23$) to 1800 ($R^* = 2.0$) with an acceleration $dR^*/dt = 0.004$. Figure 2 shows the (ϕ, θ)-plane distributions of the same integrated azimuthal vorticity component as in Figure 1, plus a slice of

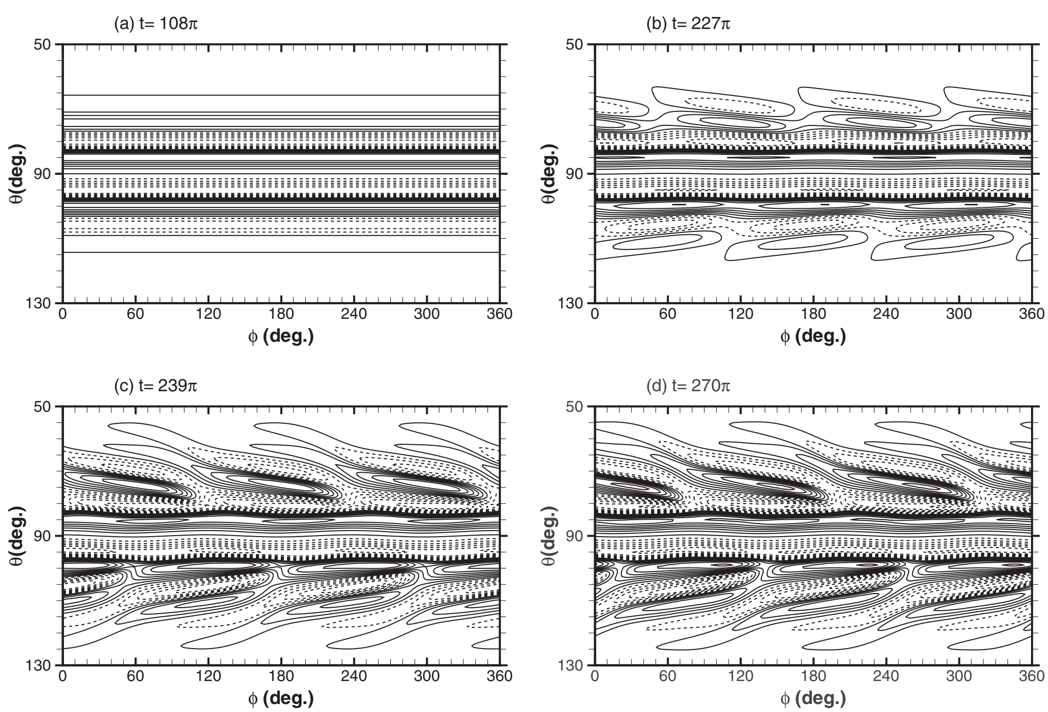

FIG. 1. (ϕ, θ)-plane distributions of the azimuthal vorticity component at four different times in the formation process of the spiral TG vortex flow IITS($T = 1$, $S_P = 3$) for $\beta = 0.14$, Re = 1110. The quantity is integrated along the radial direction over the gap. The contour levels range from −0.12 to 0.12 in (a) and (b), and from −0.14 to 0.14 in (c) and (d), in step of 0.02. Solid lines show positive values while dashed lines show negative values.

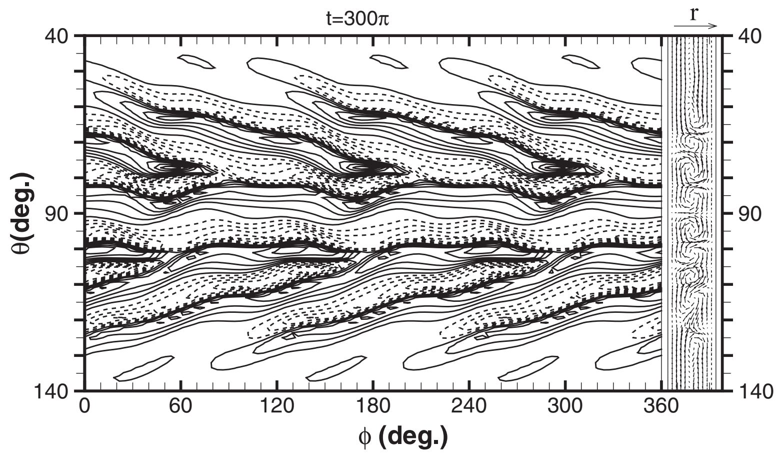

FIG. 2. (ϕ, θ)-plane distributions of the azimuthal vorticity component as in Figure 3, plus velocity vectors in one meridional plane ($\phi = 360°$) for the wavy spiral TG vortex flow IIWTS($T = 1$, $S_P = 3$, $m = 6$) for Re = 1800, $\beta = 0.14$. The contour levels range from -0.28 to 0.28 in step of 0.04.

velocity vectors in one meridional plane ($\phi = 360°$) to show the vortices. We can see that one pair of toroidal TG vortices still exist near the equator with an inflow boundary $u_r < 0$ between them, but traveling waves with wavenumber $m = 6$ are formed on the toroidal and spiral TG vortices, so the flow mode is labeled as IIWTS($T = 1$, $S_P = 3$, $m = 6$). The spiral and wavy disturbances rotate in the same direction as Ω. To analyze the frequencies, Figure 3 shows time history of the circumferential velocity component v_θ at a middle point on the equator for these two Re numbers. The oscillation is symmetric with respect to the equator for Re = 1110, but shifts south for Re = 1800. From Figure 3 we can calculate the nondimensional rotational frequency of the spiral vortices, defined

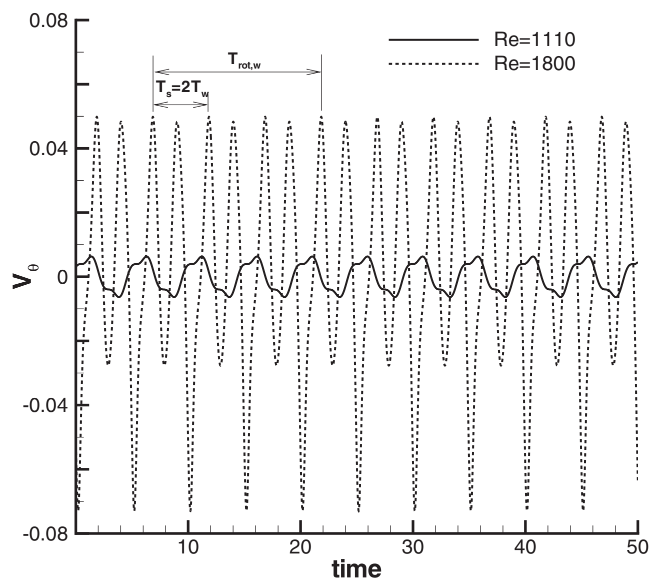

FIG. 3. Time history of the circumferential velocity component at a point $(r, \theta, \phi) = (1 + 0.5\beta, 0.5\pi, 0)$. The fundamental period of the spiral TG vortex (Re = 1110) is simply counted between every solid peak, and its rotational period is simply $T_{rot,\,s} = 3T_s$ due to $S_P = 3$. The fundamental periods T_w and T_s of the wavy spiral TG vortex flow (Re = 1800) are indicated in the graph, and the rotational period $T_{rot,w}$ of the flow is counted between every six peak intervals due to $m = 6$. Clearance ratio $\beta = 0.14$.

as $\frac{f_{rot,s}}{f} = \frac{1}{S_p}\frac{f_s}{f} = \frac{2\pi}{\tilde{T}_{rot,s}\Omega} = \frac{2\pi}{T_{rot,s}}$, and that of the traveling waves, $\frac{f_{rot,w}}{f} = \frac{1}{m}\frac{f_w}{f} = \frac{2\pi}{T_{rot,w}}$ (f being the rotational frequency of the inner sphere, f_s the fundamental frequency of spiral disturbances, and f_w that of wavy disturbances passing a fixed point in the laboratory reference frame, $S_P = 3$, $m = 6$). It is found that $\frac{f_{rot,s}}{f} = 0.427$ for Re = 1110 and $\frac{f_{rot,w}}{f} = 0.419$ for Re = 1800, respectively. These numbers are in close agreement with experimental data (cf. Figure 17 in Ref. 28).

Next, we simulate the reverse-Hopf bifurcation phenomenon of SCF which was investigated experimentally by Nakabayashi *et al.*[21] A reverse-Hopf bifurcation occurs in some nonlinear dynamical systems, which refers to the bifurcation from a limit cycle to a fixed point as the control parameter goes toward more unstable regime.

Nakabayashi *et al.*[21] observed that in the laminar-turbulent transition for $\beta < 0.2$, the flow starts from steady-state basic laminar flow, and generally goes through periodic, quasi-periodic, chaotic and fully developed turbulent states successively with increasing Re number. However, for $\beta = 0.14$, the periodicity occurring at low Re number disappears completely with increasing Re (they called this "relaminarization phenomenon," which may not be appropriate as shown at the end of this subsection), although, with a further increase of Re number, the flow becomes fluctuating again and evolves into a fully developed turbulent flow. They observed that the "relaminarization" occurred for $0.13 < \beta < 0.17$.

We directly compute the steady 2-vortex flow IIT($T = 2$) at Re = 1000 from the Stokes flow, and search for flow regimes with step of ΔRe = 10–100 and acceleration of $dR^*/dt = 0.01$–0.001 from state at previous Re. The flow becomes a wavy TG vortex flow with five traveling waves on the toroidal TG vortices (labeled as IIWT($T = 2$, $m = 5$)) at $\text{Re}_{c3} \approx 1540$. This wavy TG vortex flow remains stable for $1540 \leq \text{Re} \leq 6600$. At $\text{Re}_{c4} = 6600$, the flow returns to steady state supercritical

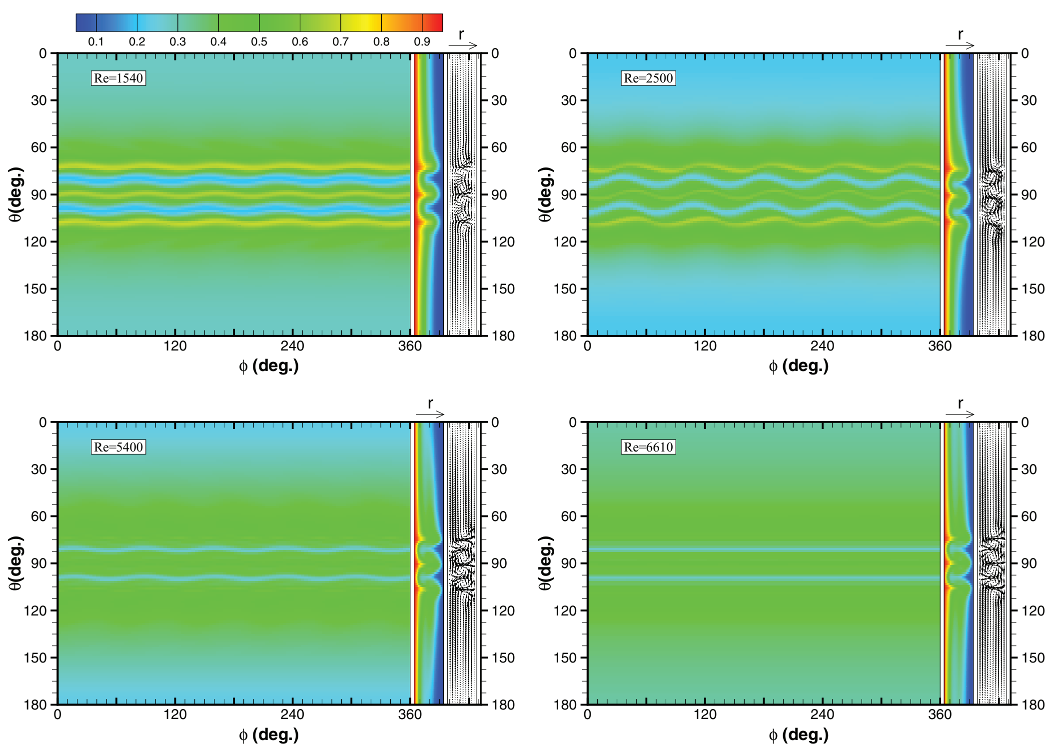

FIG. 4. Variations of the wavy TG vortex flow IITW($T = 2$, $m = 5$) with increasing Re number. For each frame, the left graph is instantaneous iso-values of the azimuthal angular velocity quantity ($\omega = v_\phi / r\sin\theta$) in the unwrapped middle spherical surface $r = (1+\beta)/2$, $0 \leq \theta \leq \pi$, $0 \leq \phi \leq 2\pi$, the middle graph is that in the meridional plane at $\phi = 2\pi$, and the right graph is velocity vectors (v_r, v_θ) in the same meridional plane. The clearance ratio $\beta = 0.14$.

2-vortex flow. Figure 4 shows the development of the flow with Re number. For each Re number, the left graph is iso-values of the azimuthal angular velocity quantity defined as $v_\phi/r\sin\theta$ in the unwrapped middle spherical surface, the middle graph is the same quantity in the meridional plane at $\phi = 2\pi$ to show the outward or inward shifting of the rotational fluid, and the right graph is the velocity vectors (v_r, v_θ) in the same meridional plane to show the vortices. We see that the amplitude of the traveling waves gets larger first with increasing Re number, but diminishes later, and finally disappears when Re > 6600. The dimensionless rotational frequencies of the traveling waves, $\frac{f_{rot,w}}{f}$, are 0.451(Re = 1540), 0.478(Re = 2500), and 0.452(Re = 5400), respectively, which are close to experimental data (cf. Figures 10 and 15 in Ref. 8). The variation of the flow mode with increasing Re number shows a change from periodic wavy TG vortex to steady TG vortex. However, the wavy TG vortex flow between Re = 1540 and 6600 is essentially laminar periodic state, so, it would be better to call the transition "reverse Hopf bifurcation" rather than "relaminarization."

B. Medium gap $\beta = 0.18$

For this medium gap, both cylinder-like disturbances such as wavy TG vortex flows in the equatorial region and secondary-flow instabilities[9] such as spiral waves in the high latitude region may occur for high Re number. The multiplicity of steady-state TG vortex flow and periodic flow at the same Re number for $\beta = 0.18$ was reported in experiment,[4] but has not been simulated numerically. In this study, we have successfully simulated the oscillating 2-vortex flow (called mode "Va" in Ref. 4) for low Re number range where supercritical steady 0- and 1-vortex flows can exist stably. This oscillating 2-vortex flow has five traveling waves, and also returns to supercritical 2-vortex flow for higher Re number, showing there is a reverse Hopf bifurcation. We have also simulated multiple TG vortex flows with shear waves for the same high Re number by imposing perturbation (1) with different values of m_a either at $t = 0$ generally, or for a short duration of the viscous diffusion time across the gap, $t_d \approx (R_2 - R_1)^2/\nu$, in some special case.

In previous axisymmetric simulation[12] for $\beta = 0.18$ and Re $\leq$ 1500, we found that the supercritical 0-vortex flow existed for 1220 $\leq$ Re $\leq$ 1500, 1-vortex flow existed for 655 $\leq$ Re $\leq$ 1500, and 2-vortex flow existed for 775 $\leq$ Re $\leq$ 1500. However, no periodic flow state was obtained for Re $\leq$ 1500. Reference 11 shown that the 0-vortex and 2-vortex flows are of the same branch, and their lower bounds in the supercritical regime are just linearly stable bounds having no relationship with dynamic bifurcations. In present three-dimensional simulation, we find that the oscillating (actually wavy) 2-vortex flow can be obtained easily for 1280 $\leq$ Re $\leq$ 2270 by direct calculation from rest or Stokes flow, and any initially steady state 2-vortex flow in the ranges of 775 $\leq$ Re $\leq$ 1280 and Re $\geq$ 2270 will become wavy once Re number is relocated in the range of [1280, 2270]. Figures 5(a) and 5(b) show the fully developed wavy 2-vortex flows at Re = 1300 and Re = 1700,

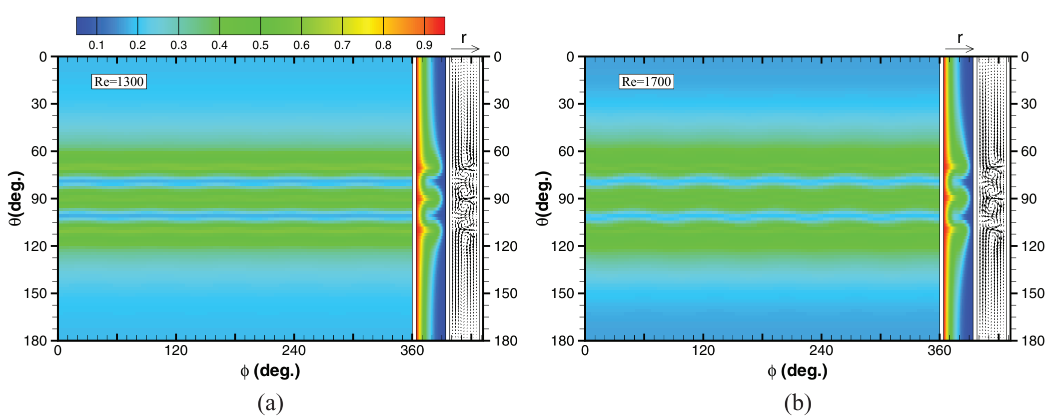

(a) (b)

FIG. 5. The same as Figure 4 but for clearance ratio $\beta = 0.18$.

respectively. Both periodic flows have five traveling waves, and the rotational frequency of the traveling waves ($\frac{f_{rot,w}}{f} = \frac{2\pi}{T_{rot,w}}$) are 0.424 (Re = 1300) and 0.420 (Re = 1700), respectively. We find that as Re number increases, the wavy TG vortex flow first occurs at $\mathrm{Re}_{c2} \approx 1280$ (Hopf bifurcation point), remains stable with respect to perturbation, and returns to the steady-state 2-vortex flow at $\mathrm{Re}_{c3} \approx 2270$ (reverse Hopf bifurcation point). On the other hand, the supercritical 0-vortex flow exists for $1470 \leq \mathrm{Re} \leq 6500$, while the steady 1-vortex flow exists from the first instability point $\mathrm{Re}_{c1} \approx 655$ up to the onset of the shear waves at $\mathrm{Re} \approx 8000$. Thus, we confirm experimental observation[4] that periodic double-vortex flow coexists with steady 0- and 1-vortex flows for $1470 \leq \mathrm{Re} \leq 2270$, and steady-state 0-, 1-, and 2-vortex flows coexist for $2270 \leq \mathrm{Re} \leq 6500$.

In the following, we present several new higher modes in region "III" for Re number that is greater than $\mathrm{Re}_{c4} \approx 6500$ but below the onset of turbulence. By using 0-, 1-, and 2-vortex flows at Re = 2500 as initial flowfields, respectively, and perturbation (1) with different numbers of m_a, multiple periodic solutions with shear waves at the same Re number can be obtained. Specifically, they are computed through linear acceleration from Re = 2500 to a Re > 6500 in dimensionless time of 60 followed by imposing perturbation (1) for one time step, or for dimensionless time of 50 for the 2-vortex with $m = 10$ case.

Figures 6(a)–6(c) show three 0-vortex flows with 7, 8, and 9 shear waves, respectively, at Re = 7200. Among them, the 8-shear wave flow is most natural to obtain: no perturbation or perturbation (1) with $m_a = 1$, 2, 4–6, 8, 10–18 can lead to it. It is remarked that this flow pattern corresponds to the non-axisymmetric instabilities with 8 wavenumbers in Fig. 3 of Ref. 29. The 7-shear wave flow can be obtained with $m_a = 7$, and the 9-shear wave flow can be obtained with

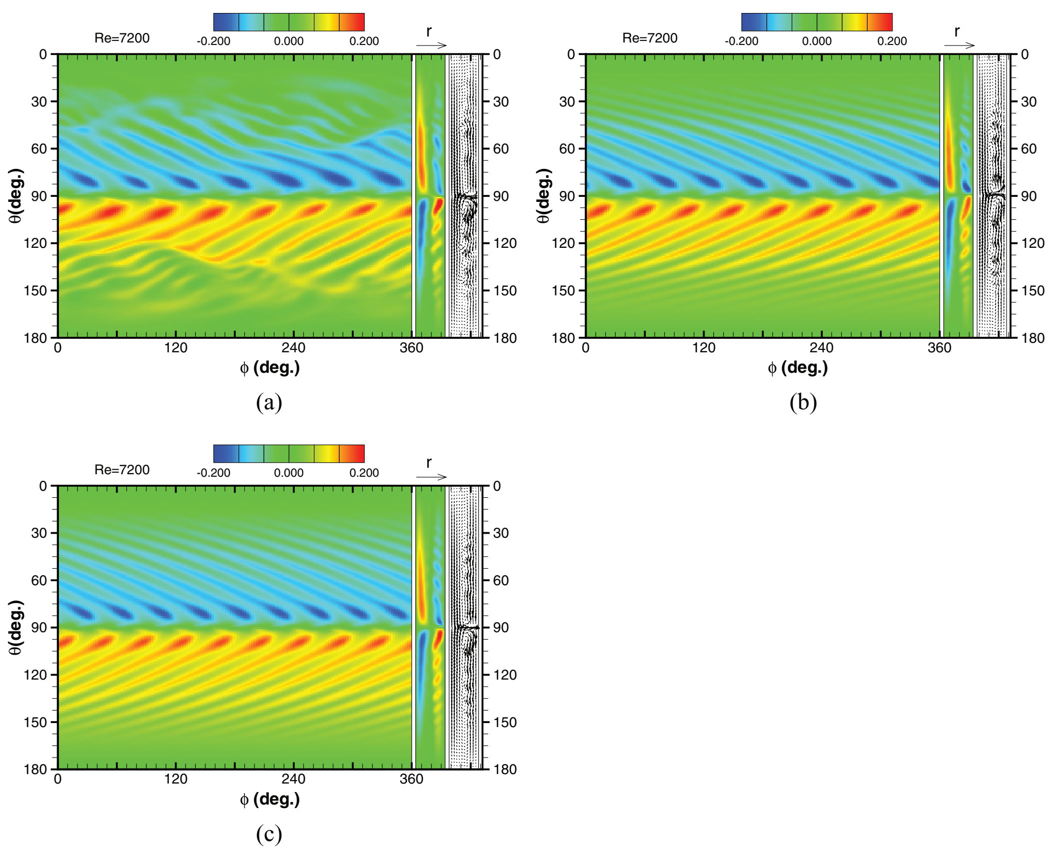

(a) (b) (c)

FIG. 6. Multiple 0-vortex flows with different numbers of shear waves at Re = 7200 for clearance ratio $\beta = 0.18$. For each frame, the left graph is instantaneous iso-values of the circumferential velocity component v_θ in the unwrapped spherical surface $r = 1 + 0.7\beta, 0 \leq \theta \leq \pi, 0 \leq \phi \leq 2\pi$, the middle graph is that in the meridional plane at $\phi = 2\pi$, and the right graph is velocity vectors (v_r, v_θ) in the same meridional plane. (a) 7 shear waves; (b) 8 shear waves; (c) 9 shear waves.

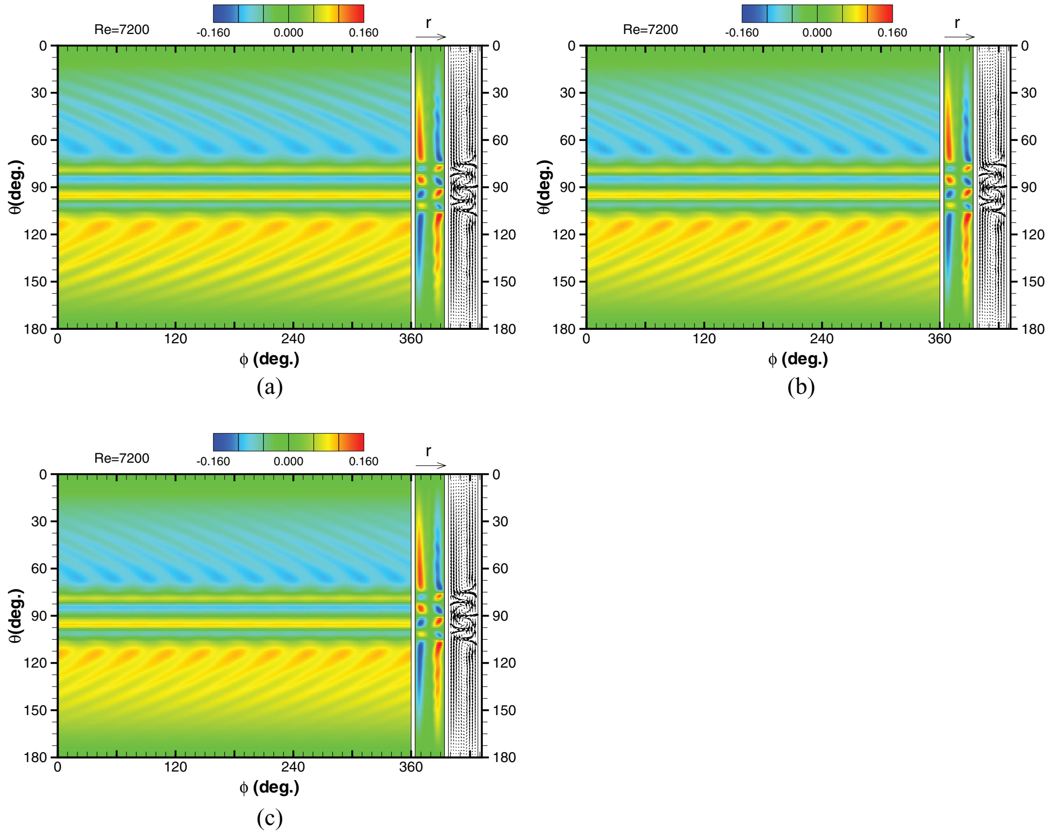

FIG. 7. The same as Figure 6 but for multiple 2-vortex flows with different numbers of shear waves. (a) 8 shear waves; (b) 9 shear waves; (c) 10 shear waves.

$m = 3$ or 9, both of which need a moderate amount of amplitude $\varepsilon_1 = 10^{-4}$. The 7-shear waves appear to be quasi-periodic while the 8- and 9-shear waves are fully periodic flows. The outflow boundary at the equator is wavy due to the influence of the shear waves. The shear waves look like spiral vortices as shown Figure 2, but they do not have vortex cells across the whole gap width, which would appear for $\beta = 0.14$ (this can be seen from the velocity vectors in Figure 2). They are formed near the outer sphere due to the viscous cross-flow instability.[9,13] Similar shear waves were also found in a wider gap by Araki[18] (they called it spiral waves). We note that the shear waves remain stable even after two hundreds of inner sphere rotation, but will change into chaotic state at slightly higher Re number. Therefore, the shear wave flows at Re = 7200 can be categorized to the transitional flow regime “III.”

Figures 7(a)–7(c) show three 2-vortex flows with 8, 9, and 10 shear waves, respectively, at Re = 7200, where the 9-shear wave flow is most natural to obtain. The 8-shear wave flow can be obtained with $m_a = 2, 4, 8$, and the 10-shear wave flow can be obtained with $m_a = 5, 10$ for longer imposition of perturbation (1). Both of which need moderate amplitudes like $\varepsilon_1 = 10^{-4}$, and very larger values like $\varepsilon_1 = 10^{-2}$ or very small values like $\varepsilon_1 = 10^{-12}$ often make the flow develop into the default 9-shear wave flow irrespective of what m_a. The 9-shear wave flow can be obtained without perturbation or with perturbation with $m_a = 1, 3, 6, 7, 9$ as well as other integer numbers that are not divisors of 8 or 10. We observe that the outflow boundaries of the TG vortices are wavy due to the influence of the shear waves away from the equator, but remain toroidal near the equator. As Re number is increased further, the 2-vortex flow with shear waves will change into 1-vortex flow with massively chaotic flow in the secondary flow region, and finally to turbulence.

On the other hand, the 1-vortex flow is more stable than the 0- and 2-vortex flows in that it has no spiral disturbances developed at Re = 7200. We have used both 34 × 360 × 153 and 34 × 480 × 257 grids to obtain the same conclusion. Figures 8(a)–8(c) show multiple 1-vortex flows

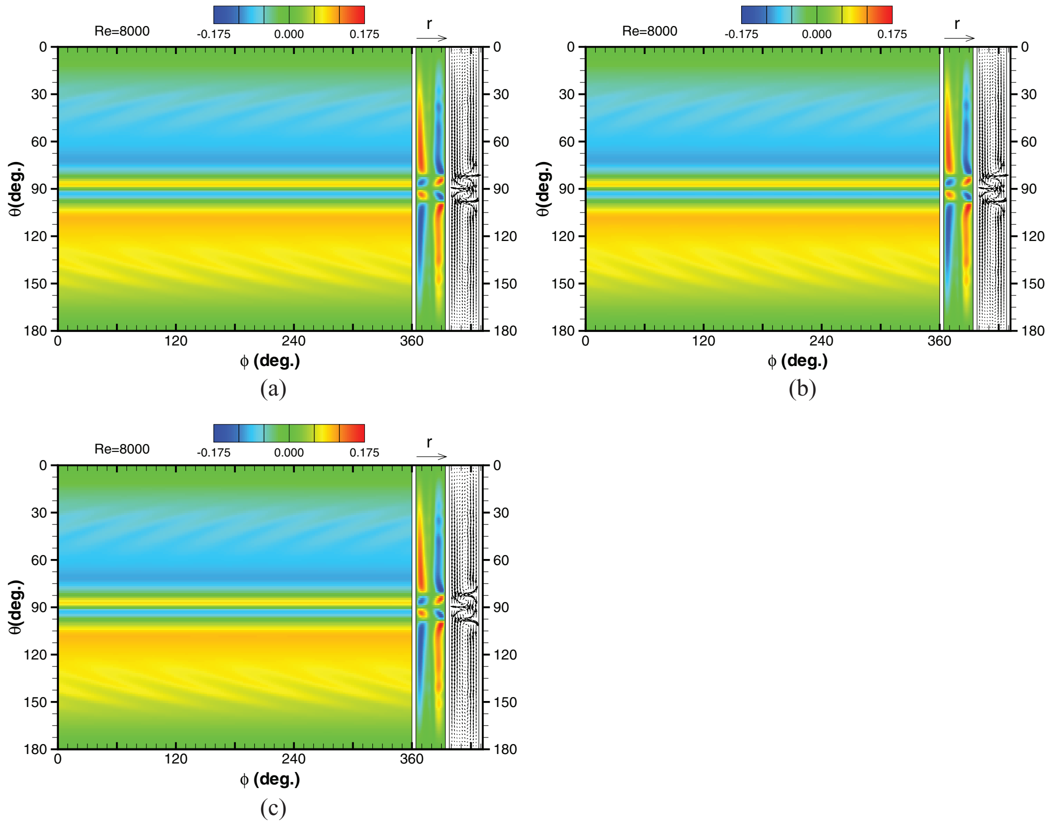

FIG. 8. The same as Figure 6 but for multiple 1-vortex flows with different numbers of shear waves at Re = 8000. (a) 5 shear waves; (b) 6 shear waves; (c) 6:5 shear waves.

with three different shear-wave patterns at Re = 8000. It is seen that the shear waves have clockwise spirals from high latitude region to low latitude region when viewed from top of the north pole, and both the inflow and outflow boundaries of the TG vortices remain almost parallel to the equator. The spirals are different from the counterclockwise spirals as occurred in 0- and 2-vortex flows. The 5-shear wave flow seems to be the default for Re = 8000: if perturbation (1) is not imposed or imposed with $m_a = 1, 4, 5, 7–9$, then the flow goes to the 5-shear wave after long time evolution. If $m_a = 2, 3, 6$, then the flow goes to the 6-shear wave. An interesting case is when $m_a = 11$, the flow goes to one with 5-shear waves in one hemisphere and 6-shear waves in the other hemisphere (Figure 8(c)). All the flows are basically periodic but contain non-periodic fluctuations between the periodic fluctuations. A more subtle difference is that the north and south shear waves may be in phase or in differential phase. These reflect the intricate nature of the multiple solutions of the SCF.

Finally, Table I summarizes rotational frequencies of the multiple TG vortex flows with different shear waves for clearance ratio $\beta = 0.18$. It is remarked that the spiral waves of the 1-vortex flows move very slowly in the same direction of the inner sphere rotation.

TABLE I. Nondimensional rotational frequencies of TG vortex flows with shear waves for $\beta = 0.18$.

Re	Baseline TG vortex flow	Rotational frequency $f_{rot,\,sh}$ (wavenumber S_{H})		
7200	0-vortex	0.523 (7)	0.524 (8)	0.522 (9)
7200	2-vortex	0.478 (8)	0.476 (9)	0.470 (10)
8000	1-vortex	0.00821 (5)	0.0571 (6:5)	0.0478 (6)

IV. CONCLUSIONS

The spiral and wavy disturbances of the flow between two concentric spheres with the inner one rotating and the outer one stationary are investigated numerically for two gap widths ($\beta = 0.14$ and 0.18) for a wide range of Reynolds numbers. The numerical simulation is based on solving the three-dimensional incompressible Navier-Stokes equations with a fifth-order upwind compact method. For $\beta = 0.14$, the computation reproduces the occurrence of the spiral Taylor-Görtler vortices at Re $= 1110$ as in literature. Furthermore, a Hopf bifurcation at $\mathrm{Re}_{c3} = 1540$ for which the steady 2-vortex flow develops into a wavy one, and corresponding reverse Hopf bifurcation at $\mathrm{Re}_{c4} = 6600$ for which the periodic wavy TG vortices change back to steady toroidal TG vortices, are found.

For $\beta = 0.18$, the present simulation reproduces Wimmer's experimental observation that steady flows can coexist with periodic flows at the same Reynolds number. The supercritical steady 0-, 1-, and 2-vortex flows can coexist for $2270 \leq \mathrm{Re} \leq 6500$. The steady 0- and 2-vortex flows first lose stability to spiral disturbances (shear waves) in the secondary flow region for Re ≥ 6500. On the other hand, the steady 1-vortex flow does not experience any wavy or spiral disturbance up to Re ≈ 8000, where it loses stability to spiral disturbances with fewer wavenumbers in the secondary flow region but still remains toroidal near the equator. It is found that the multiple higher modes can be obtained by using the proposed perturbation with different wavenumbers. These flow modes are described in terms of rotational frequency, wave number, and spatial structure. The multiplicity in certain range of Reynolds numbers reflects a nature of rotating fluid constrained in spherical annulus.

ACKNOWLEDGMENTS

This work was supported by state key program for developing basic sciences (Grant No. 2010CB731505) and National Natural Science Foundation of China (Grant Nos. 10972230 and 11021101).

[1] M. Wimmer, "Viscous flow and instabilities near rotating bodies," Prog. Aerospace Sci. **25**, 43–103 (1988).
[2] O. Sawatzki and J. Zierep, "Das Stromfeld im Spalt zwichen zwei konzentrischen Kulgelflachen, von denen die innere rotiert," Acta Mech. **9**, 13–35 (1970).
[3] B. Munson and M. Menguturk, "Viscous incompressible flow between concentric rotating spheres. Part 3. Linear stability," J. Fluid Mech. **69**, 281–318 (1975).
[4] M. Wimmer, "Experiments on a viscous fluid flow between concentric rotating spheres," J. Fluid Mech. **78**, 317–335 (1976).
[5] I. Yavorskaya, Yu. Belyaev, A. Monakhov, N. Astaf'eva, S. Scherbakov, and N. Vvedenskaya, "Stability, nonuniqueness and transition to turbulence in the flow between two rotating spheres," Report No. 595, Space Research Institute of the Academy of Science, USSR, 1980.
[6] F. Bartels, "Taylor vortices between two-concentric rotating spheres," J. Fluid Mech. **119**, 1–65 (1982).
[7] K. Nakabayashi, "Transition of Taylor-Görtler vortex flow in spherical Couette flow," J. Fluid Mech. **132**, 209–230 (1983).
[8] K. Nakabayashi and Y. Tsuchida, "Flow-history effect on higher modes in the spherical Coutte flow," J. Fluid Mech. **295**, 43–60 (1995).
[9] K. Bühler and J. Zierep, "Dynamical instabilities and transition to turbulence in spherical gap flows," in *Proceedings of the 1st European Turbulence Conference on Advances in Turbulence*, edited by G. Comte-Bellot and J. Mathieu (Springer, Berlin, 1987), p. 16.
[10] G. Schrauf, "The first instability in spherical Couette flow," J. Fluid Mech. **166**, 287–303 (1986).
[11] P. Marcus and L. Tuckerman, "Simulation of flow between two concentric rotating spheres. Part 1: Steady states," Fluid Mech. **185**, 1–30 (1987); "Simulations of flow between two concentric rotating spheres. Part 2: Transitions," *ibid.* **185**, 31–65 (1987).
[12] L. Yuan, D. X. Fu, and Y. W. Ma, "Numerical study of bifurcation solutions of spherical Taylor-Couette flow," Sci. China Ser. A **39**(2), 187–196 (1996).
[13] K. Nakabayashi, Y. Tsuchida, and Z. Zheng, "Characteristics of disturbances in the laminar-turbulent transition of spherical Couette flow. 1. Spiral Taylor-Görtler vortices and traveling waves for narrow gaps," Phys. Fluids **14**(11), 3963–3972 (2002).
[14] K. Nakabayashi, Z. Zheng, and Y. Tsuchida, "Characteristics of disturbances in the laminar-turbulent transition of spherical Couette flow. 2. New disturbances observed for a medium gap," Phys. Fluids **14**(11), 3973–3982 (2002).
[15] G. Dumas and A. Leonard, "A divergence-free spectral expansions method for three-dimensional flows in spherical-gap geometries," J. Comput. Phys. **111**, 205–219 (1994).
[16] C. Egbers and H. Rath, "The existence of Taylor vortices and wide-gap instabilities in spherical Couette flow," Acta Mech. **111**, 125–140 (1995).
[17] O. Zikanov, "Symmetry-breaking bifurcations in spherical Couette flow," J. Fluid Mech. **310**, 293–324 (1996).
[18] K. Araki, J. Mizushima, and S. Yanase, "The nonaxisymmetric instability of the wide-gap spherical Couette flow," Phys. Fluids **9**, 1197–1199 (1997).

[19] P. Wulf, C. Egbers, and H. Rath, "Routes to chaos in wide-gap spherical Couette flow," Phys. Fluids **11**, 1359–1372 (1999).
[20] W. M. Sha and K. Nakabayashi, "On the structure and formation of spiral Taylor-Görtler vortices in spherical Couette flow," J. Fluid Mech. **431**, 323–345 (2001).
[21] K. Nakabayashi, W. M. Sha, and Y. Tsuchida, "Relaminarization phenomena and external-disturbance effects in spherical Couette flow," J. Fluid Mech. **534**, 327–350 (2005).
[22] O. Ladyzhenskaya, "Mathematical analysis of Navier-Stokes equations for incompressible liquids," Ann. Rev. Fluid Mech. **7**, 249–272 (1975).
[23] C. Mamun and L. Tuckerman, "Asymmetry and Hopf bifurcation in spherical Couette flow," Phys. Fluids **7**(1), 80–91 (1995).
[24] L. Yuan, "Numerical study of multiple periodic flow states in spherical Taylor-Couette flow," Sci. China Ser. A **47**, S81–S91 (2004).
[25] A. Shah and L. Yuan, "Flux-difference splitting-based upwind compact schemes for the incompressible Navier-Stokes equations," Int. J. Numer. Meth. Fluids **61**(5), 552–568 (2009).
[26] L. Yuan, H. Guo, and Z. H. Yin, "On optimal message vector length for block single parallel partition algorithm in a three-dimensional ADI solver," Appl. Math. Comput. **215**, 2565–2577 (2009).
[27] W. Schroeder and H. Keller, "Wavy Taylor-vortex flows via multigrid-continuation methods," J. Comput. Phys. **91**(1), 197–227 (1990).
[28] K. Nakabayashi and Y. Tsuchida, "Spectral study of the laminar-turbulent transition in spherical Couette flow," J. Fluid Mech. **194**, 101–132 (1988).
[29] R. Hollerbach, M. Junk, and C. Egbers, "Non-axisymmetric instabilities in basic state spherical Couette flow," Fluid Dyn. Res. **38**, 257–273 (2006).